Tôhoku Geophys. Journ. (Sci. Rep. Tôhoku Univ., Ser. 5), Vol. 37, No. 2, pp. 91-108, 2006

2-D imaging of the lower mantle structure beneath South Africa estimated from shear wave multiphase analysis

MUNGIYA KUBANZA[a,*], HIROYUKI HAMAGUCHI[b,**]

(Received April 4, 2006; accepted June 2, 2006)

Abstract: We investigated the velocity structure of the lower mantle beneath South Africa based on analysis of the shear waveform data collected from the IRIS Data Management Center. Among the 26 events with depths greater than 50 km and body wave magnitude greater than or equal to 5.5, three events with the high quality of seismograms were retained in this study. We analyzed 18 ScS-S, 53 S-SKS and 46 SKKS-SKS differential travel times measured by cross-correlation, in addition to 71 S, 18 ScS, 53 SKS and 46 SKKS absolute travel times. These are ascertained from the combination of the South Sandwich and the South American events with the temporary arrays of broadband seismic stations that are deployed in Eastern Africa (Tanzania) and South Africa (Kaapvaal), including stations BGCA and SUR of IRIS Global Seismographic Network. Large travel-time delays greater than 10 seconds of shear waves are observed with reference to the PREM, and these delays increase gradually with epicentral distances, implying that the seismic phase propagates through an extremely low S-wave velocity region in the lower mantle. Directly comparing the observed travel times with the predicted ones deduced from the 3-D S-wave velocity models such as SKS12WM13, we find broad low-velocity region of 3% S-wave velocity reduction in a deeper part of the lower mantle (800 km above the core mantle boundary (CMB)) beneath the Southwestern Africa to the Southeastern Atlantic Ocean. This spatial pattern suggests an existence of a broad upwelling plume from the CMB beneath the above mentioned region.

Keywords: shear waves, lower mantle, heterogeneity, CMB, mantle plume, Africa

1 Introduction

Knowledge of the seismic structure of the lower mantle under the African continent and its surrounding regions is important for our understanding of hotspot volcanism and the origin of mantle plumes. Recently, geophysical and geological reviews and classification of hotspots have been attempted. The viewpoints on hotspots vary gradually with increasing new observations and analysis, however, a hotspot-mantle plume hypothesis is still open for discussion (Steinberger and O'Connell, 1998; Steinberger, 2000; Zhao, 2001; Zhao, 2004; Ritsema and Allen, 2003; Courtillot *et al.*, 2003). A

[a] Department of Geophysics, Graduate School of Science, Tohoku University, Aramaki-aza Aoba, Aoba-ku, Sendai 980-8578, JAPAN.
[b] Research Center for Prediction of Earthquakes and Volcanic Eruptions, Graduate School of Science, Tohoku University, Aramaki-aza Aoba, Aoba-ku, Sendai 980-8578, JAPAN.
* Corresponding author. Tel.: +81-22-795-6531; Fax: +81-22-795-6783.
E-mail address: kubanza@zisin.geophys.tohoku.ac.jp (M. Kubanza)
** Retired

prominent low-velocity anomaly in the lower mantle beneath Africa has been imaged in all the seismic tomographic models (Liu and Dziewonski, 1994 ; Ritsema *et al.*, 1999 ; Castle *et al.*, 2000 ; Megnin and Romanowicz, 2000 ; Zhao, 2001 ; Zhao, 2004). Such a low-velocity anomaly is interpreted as evidence for the existence of a superplume, that is a huge upwelling from the CMB.

Until the 1990s, the small number of seismic stations in Africa had prevented the examination of the deep structure beneath Africa. There were only a few studies investigating the lower mantle beneath Africa and its surrounding regions (Lavely *et al.*, 1986 ; Tanaka and Hamaguchi, 1992). However, in recent years, the number of permanent stations has increased and temporary observations have been conducted with dense seismic arrays. Therefore recent deployment of broadband seismic stations in Africa leads the advance of understanding the deep structure of Africa and its surrounding regions. The seismic data obtained from the IRIS/PASSCAL experiments provide a valuable data set (Nyblade *et al.*, 1996 ; Nyblade and Langston, 2002).

Ritsema *et al.* (1998) showed that a low-velocity region extends obliquely from the CMB about 1,500 km up to the mantle beneath Southern Africa by forward modeling. Ni *et al.* (1999) and Ni and Helmberger (2001a, 2003a, b) showed that the low-velocity region beneath Southwestern Africa extends 1,200-1,500 km above the CMB. Helmberger *et al.* (2000) and Ni and Helmberger (2001b) detected ultra-low velocity zones beneath Eastern African Rift and Iceland.

These recent studies proposed individually a similar shape of the low-velocity region extending 1,500 km above the CMB by using various data sets consisting of classical analog data and modern digital data. However, the models proposed to the nearly same region beneath Africa have not been crosschecked. Therefore it is not clear whether these models are consistent with each other or not. In this study we focus on the Southern Africa-Atlantic region and investigate the shear wave velocity structure by using the crisscrossing rays that pass through the lower mantle.

2 Data

The data are concerned only with events with focal depths greater than 50 km and body wave magnitude greater than or equal to 5.5 during the period of 1990 to 1999. We made a list of 26 events located in South America, South Sandwich Islands and the Western Pacific Ocean. Among them three events met the criterion of a high signal-to-noise ratio and impulsive signals. All the waveform data from the three events were obtained from the Data Management Center (DMC) at the Incorporated Research Institutions for Seismology (IRIS). Table 1 shows the hypocentral parameters for the three events used in the present study. Fig. 1a displays the geographical distribution of the events, seismic stations and ray paths geometry, including the ScS bounce points at the CMB (at 2,891 km in depth), the SKS and the SKKS transmission points at the CMB and the S transmission points at the top of D″ layer (at 2,741 km in depth). Fig. 1b is the enlargement of the crisscrossing rays at the lower mantle beneath South Africa where

Table 1. Hypocentral parameters of the earthquakes used in this study

Event No.	Date Y/M/D	Origine time H : M : S	Latitude (deg)	Longitude (deg)	Depth (km)	m_b	Corresponding seismic stations
E1*	1994/07/25	22 : 00 : 22.98	−56.362	−27.365	81.3	6.3	Tanzania array
E2**	1994/10/20	01 : 15 : 16.18	−39.190	−70.800	164.0	5.8	Tanzania array, BGCA
E3***	1997/09/02	12 : 13 : 22.92	3.849	−75.749	198.7	6.5	Kaapvaal array, SUR

Data are taken from the Preliminary Determination of Epicenters.
Stars indicate the earthquake geographical region (Young *et al.*, 1996)
*South Sandwich Islands
**Southern Argentina
***Colombia

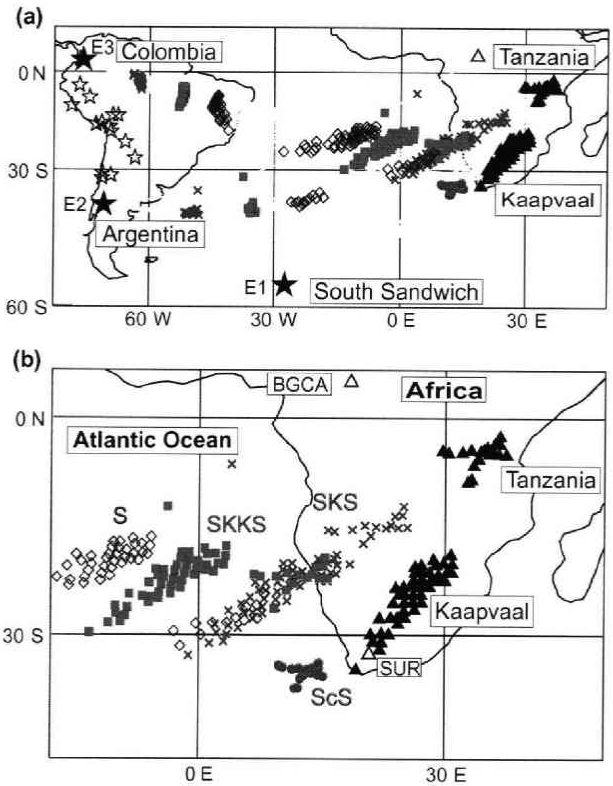

Fig. 1. Map showing the study region. (a) Distribution of ray paths connecting events (open- and solid-stars) and stations (open- and solid-triangles) used in this study. Solid stars denote events used in the analysis and open stars show the events investigated but not used. Pink circles denote the ScS bounce points at the core-mantle boundary (CMB). Crosses and green squares are the SKS and SKKS transmission points at the CMB, respectively. Open diamonds indicate the S transmission points at the top of D″ layer. E1, E2 and E3 are events numbers listed in Table 1. (b) Zoom map showing the exit points of the target phases: S (open diamonds) at the top of D″ layer, SKS (crosses) and SKKS (green squares) from the CMB and ScS (pink circles) bounce points at the CMB. Open- and solid-triangles denote the seismic stations used.

the S and the SKKS exit points from the Argentina event and the SKS exit points from the Colombia event are clearly overlapped.

3 Procedure

The absolute arrival times among the S, ScS, SKS, and SKKS seismic phases were read carefully by eye-picking. The differential travel times between the arrivals of two target phases were determined by using the cross-correlation method after an appropriate correction of waveforms when necessary (see section 3.3). The ScS-S times are measured on the transverse components, and the S-SKS and SKKS-SKS times are obtained on the radial components.

3.1 S and ScS travel times

We obtained the absolute arrival times and the differential travel times of ScS-S from the South Sandwich event recorded by the Tanzania broadband seismic array.

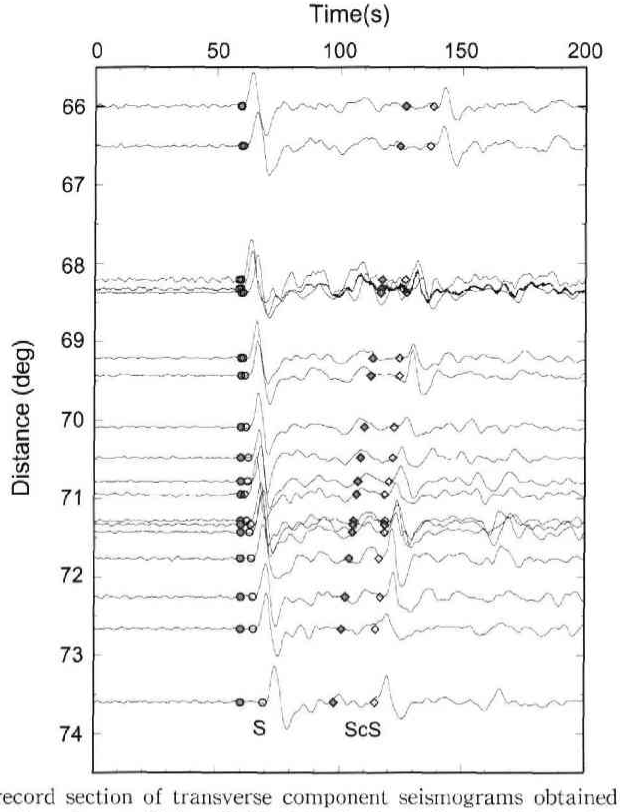

Fig. 2. A record section of transverse component seismograms obtained from the combination of event E1 (see Table 1) in the South Sandwich Islands and broadband seismic stations at Tanzania array. Solid-circles and solid-diamonds are the theoretical S and ScS arrival times with respect to PREM, respectively. Open-circles and open-diamonds indicate the observed S and ScS onsets, respectively. Seismograms are aligned on the theoretical S arrival time.

The observations cover the epicentral distance ranges of 65° to 74° for which S and ScS phases are clearly identifiable. Fig. 2 shows a record section of the transverse component of the event E1 (see Table 1) as aligned on the predicted S arrival time for the Preliminary Reference Earth Model (PREM) (Dziewonski and Anderson, 1981). We applied the ellipticity correction (Kennett and Gudmundsson, 1996) on both phases. Observed and predicted times are marked as open and solid symbols in Fig. 2, respectively. The observed onset times of S phase are close to the predicted times by PREM producing nearly zero residuals at range from 66° to 69° and then become increasingly delayed at the larger range. However the ScS is delayed with nearly constant offset over the entire range of the observations.

3.2 S, SKS and SKKS travel times

The S-SKS and SKKS-SKS observations including their absolute arrival times are

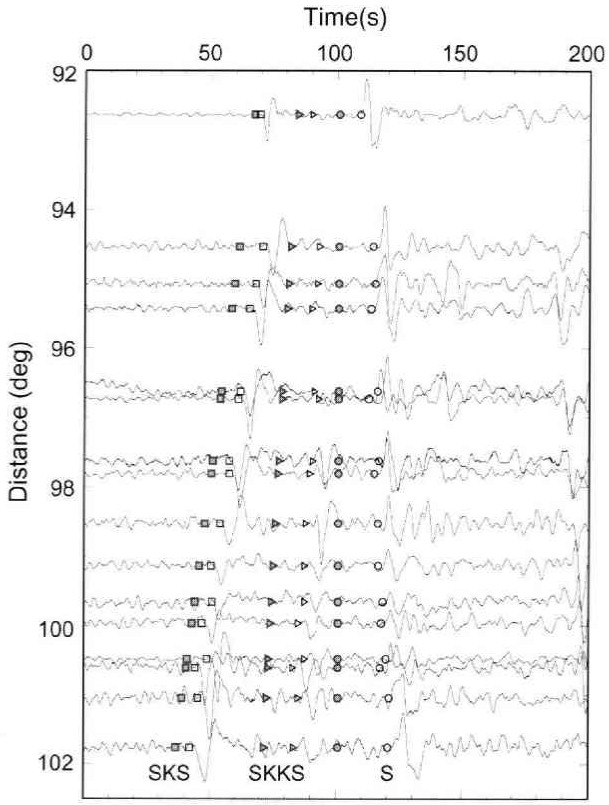

Fig. 3. A record section of the radial component seismograms obtained from the combination of event E2 (see Table 1) in the Southern Argentina and broadband stations at Tanzania array and station BGCA of IRIS/GSN in Central Africa. Solid-squares, solid-triangles and solid-circles denote the theoretical SKS, SKKS and S arrival times with respect to PREM, respectively. Open-squares, open-triangles and open-circles indicate the observed SKS, SKKS and S onsets, respectively.

obtained from seismograms of the events in South America (Argentina and Colombia). Fig. 3 shows a record section of the radial component seismograms of event E2 (see Table 1) recorded at the Tanzania array and a station BGCA of IRIS/GSN network. The predicted arrival times of the S, SKS and SKKS phases were calculated using PREM and are plotted on the seismograms as solid symbols after applying the ellipticity correction. Open symbols denote the observed arrival times. The SKS offset with respect to PREM decreases with increasing distance while the S offset increases with distance and the SKKS offset shows nearly a constant value over the entire range (92°-102°), except for some isolated points.

Fig. 4 shows the radial component seismograms of event E3 (see Table 1) recorded at the Kaapvaal array and a station SUR of IRIS/GSN in South Africa. The seismograms are aligned on the predicted S arrival time. SKS and SKKS offsets with respect to PREM increase slightly with increasing distance through the entire range (96°-107°). However the S phase shows a different pattern of offsets, showing early arrivals at a shorter distance (96°-101°), close arrivals to PREM in the middle (102°-103°) and gradu-

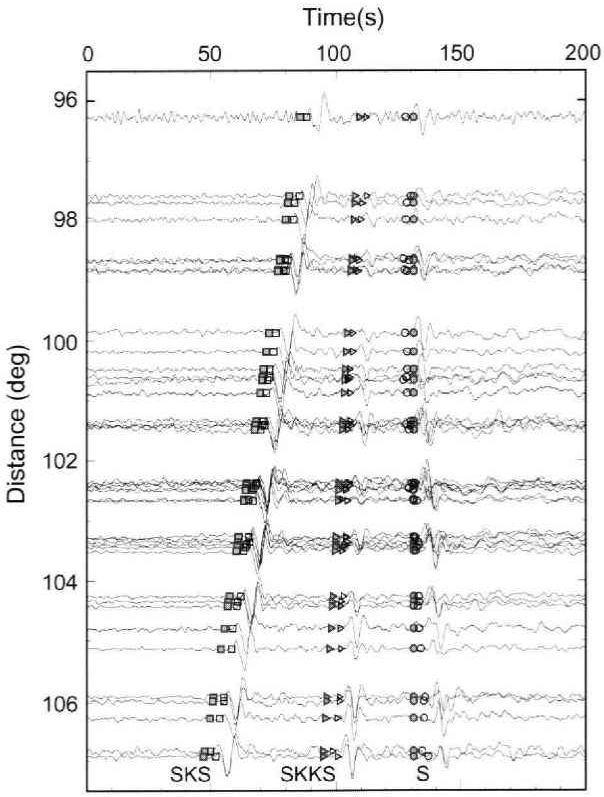

Fig. 4. A record section of radial component seismograms obtained from the combination of event E3 (see Table 1) in Colombia and broadband stations at Kaapvaal array and station SUR of IRIS/GSN in South Africa. Solid and open symbols denote theoretical and observed arrival times of SKS, SKKS and S phases, respectively.

ally increase with distance at larger range ($>104°$).

3.3 Cross-correlation of waveforms

We measure the ScS-S, S-SKS and SKKS-SKS differential travel times by using the waveforms cross-correlation method. This method is widely used to measure the differential travel times between two seismic phases (e.g. Lavely *et al.*, 1986; Tanaka and Hamaguchi, 1992). Fig. 5a is an example of the ScS-S differential travel time measurement. Using the cursor on a PC display, we pick up an onset of the S phase and set a successive time window of 20 seconds from this onset. We calculate the cross-correlation coefficient between the S phase and the seismic waves following the S phase. The maximum cross-correlation coefficient in the vicinity of ScS phase can be adopted as the observed differential travel time between both phases. We determine the onset of the ScS phase by stacking the obtained differential travel time to the observed onset time of the S phase. The S phase within the appropriate time window is then shifted to match with the ScS phase.

Fig. 5b shows the measurement of the S-SKS differential travel times. The process to measure the S-SKS times is the same manner, except that the SKS onset is picked, as the first arrival. The SKS phase is shifted to match with the S phase. Because of polarity reversal of SKS against S, we consider the maximum negative correlation coefficient in the vicinity of the S phase to measure the time difference between both phases.

The SKKS-SKS differential travel time measurements (Fig. 5c) require the establishment of Hilbert transform (Choy and Richards, 1975) because of their waveform characteristics. First, we determine the time window of 20 seconds to sample the SKS phase. Next, we apply the Hilbert transform to SKS phase resulting a waveform that resembles to SKKS phase with polarity reversal as H (SKS)=-SKKS. Except for this additional operation, the process to measure the SKKS-SKS differential travel times remains same as the case of S-SKS. SKS phase is then shifted to match with the SKKS phase.

3.4 Results of measurements

We retain measurements with an absolute value of correlation coefficients greater than or equal to 0.7 as the best data and those between 0.6 and 0.7 as good data. All the measurements with the correlation coefficients less than 0.6 are rejected. As explained above the travel times of S, ScS, SKS and SKKS are corrected for the Earth's ellipticity and residuals of the differential and absolute travel times are calculated by using the PREM. We obtained 18 differential travel times for ScS-S, 53 for S-SKS, 46 for SKKS-SKS, and 71 absolute travel times for S, 18 for ScS, 53 for SKS and 46 for SKKS. We found anomalously large time delays greater than 10 seconds with respect to PREM. These delays increase gradually with epicentral distances, suggesting an evidence of strong S-wave velocity variations in the lower mantle beneath South Africa.

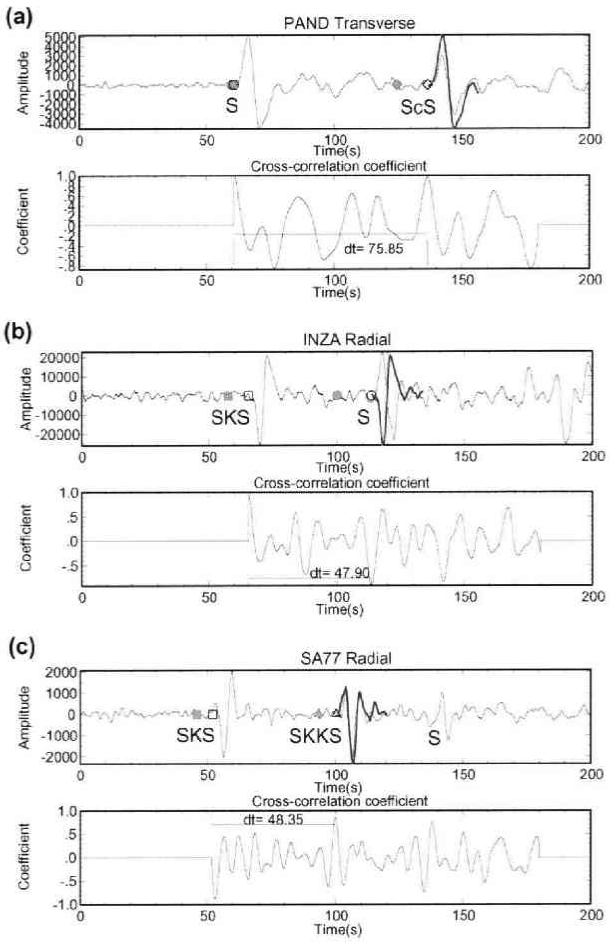

Fig. 5. Examples of differential travel time measurement by cross-correlation method. (a) (Top) The transverse component of seismogram of the event E1 (see Table 1) in South Sandwich Islands recorded at station PAND of Tanzania array. Gray-circle and gray-diamond are the PREM predicted arrival times of S and ScS phases, respectively. Open-circle and open-diamond indicate the observed S and ScS onsets. S phase is sampled with an appropriate time window of 20 seconds and is shifted to match with the ScS phase. (Bottom) Correlation coefficient as a function of time. *dt* indicates the measured differential travel times between S and ScS phases. This measurement has a cross-correlation coefficient of 0.97, indicative of high quality observation. (b) Example of S-SKS measurement on a radial component seismogram recorded at station INZA of Tanzania array. This measurement has a cross-correlation coefficient of -0.91. See text for details. (c) Same as (b) but the measurement concerns the SKKS-SKS observed at station SA77 of Kaapvaal array. This measurement has a cross-correlation coefficient of 0.86.

3.5 Travel time predictions from the 3-D S-wave heterogeneity models

The ray path of the seismic phases is traced through the PREM and that ray path is divided into ray segments through the layers of the Earth. The travel time anomalies

resulting from the 3-D heterogeneity are calculated by taking an integration of velocity perturbations along a ray path traced through PREM such as

$$\delta t^{model} = -\int_{path} \frac{\delta v}{V} dt, \tag{1}$$

where δt is the travel time perturbation from a given 3-D model; δv is the velocity perturbation from the 3-D model; V is the velocity from PREM at a corresponding depth; dt is the travel time increment, and *path* is the integration path corresponding to the ray path in the mantle.

3.6 Comparison between observed and predicted times from the 3-D models

We compare the residuals of the absolute and differential travel times with those predicted from the 3-D S-wave velocity models in the mantle: SKS12WM13 (Liu and Dziewonski, 1994), S12WM13 (Su *et al.*, 1994), S20RTS (Ritsema *et al.*, 1999) and SB4L18 (Masters *et al.*, 2000). Fig. 6 compares the observed data with the predicted ones from those 3-D mantle models for the South Sandwich event. Open symbols show the observed data and the solid symbols show the predicted times. We found that these 3-D mantle models except the model SKS12WM13 (solid circles) can not explain the data set from the South Sandwich earthquake. Fig. 7 illustrates the absolute and differential time residuals versus epicentral distances for S-wave and S-SKS for the Argentina event. Large time delays greater than 10 seconds for S-wave increase gradually with epicentral distances (open diamonds in Fig. 7a), suggesting that this seismic phase propagated through an extremely low-velocity region. Large variations of differential travel time residuals in S-SKS (open circles in Fig. 7b) indicate that strong S-wave velocity variations exist in the lower mantle beneath Africa.

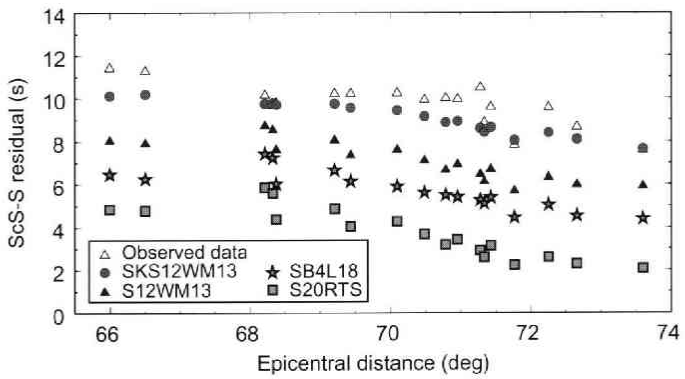

Fig. 6. Residuals of ScS-S differential travel times with respect to PREM as a function of epicentral distance for the South Sandwich event. The solid symbols are the residuals predicted by using the 3-D S-wave velocity models. Model SKS12WM13 produces residuals close to the observed data among all the 3-D models.

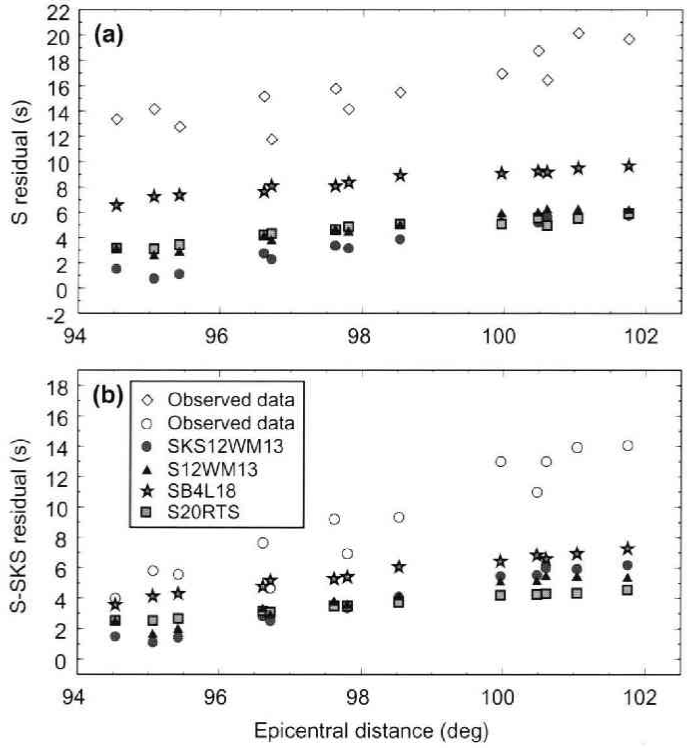

Fig. 7. Residuals of (a) S and (b) S-SKS differential travel times with respect to PREM as a function of epicentral distance for the Argentina event. The legend appended in panel (b) is also applicable to panel (a). Solid symbols have the same meaning as in Fig. 6.

4 A proposed model of shear velocity heterogeneity

To explain the discordance between the observed data and predicted ones from the 3-D shear velocity models of the Earth's mantle in Fig. 7, we modified a previous 3-D velocity model taking into consideration the crisscrossing rays emerged from the Argentina event (E2) recorded by the Tanzania array and those from the Colombia event (E3) recorded by the Kaapvaal array, respectively. Among the four 3-D models investigated in this study, SKS12WM13 gives a good explanation to our ScS-S residuals from the South Sandwich data sets (see solid circles in Fig. 6) and therefore it is taken as the model for us to improve. The modification processing includes the following steps.

First, a cross section along the ray paths connecting Colombia to Kaapvaal was considered. The shear velocity perturbation was assumed to be 3% (Ni and Helmberger, 2003a, b) and the thickness of the anomalous region was kept as a free parameter. Applying trial and error to superimpose the great-circle ray path geometry on the vertical cross-section of model SKS12WM13, the shape of the low-velocity region was systematically modified for improving the consistency between the observed and the theoretical residuals of differential and absolute times. The S-wave velocity reduction

of 3% within 800 km depth above the CMB satisfied our observed data.

Secondly, the cross-section between the Argentina event and the Tanzania array was considered, which was previously analyzed by Ni and Helmberger (2003a, b). The shape of the low velocity region was reproduced as done by Ni and Helmberger with 3% shear velocity reduction, assuming the velocity outside the model is expressed by SKS12WM13 model.

Finally, the ray paths from the Argentina event to the Tanzania array and those from the Colombia event to the Kaapvaal array were considered. We focused on the region where the exit points of the S, SKS and SKKS phases overlapped. This region locates beneath the Southeastern Atlantic Ocean within a distance range of 55°-75°. Therefore, we modified the thickness of the anomalous region estimated by Ni and Helmberger within the above distance range up to 800 km depth from the CMB, because the Colombia data set requires a thick low velocity region as described above.

Fig. 8 shows the comparison between the observed residuals and the theoretical travel time residuals based on the modified model and gives a good explanation to the absolute S residuals (Fig. 8a). An acceptable fit to the observed S SKS residuals is shown in Fig. 8b. The low-velocity region with a uniformly 3% S wave velocity reduction is projected on the geographical map as shown in Fig. 9. The selected repre-

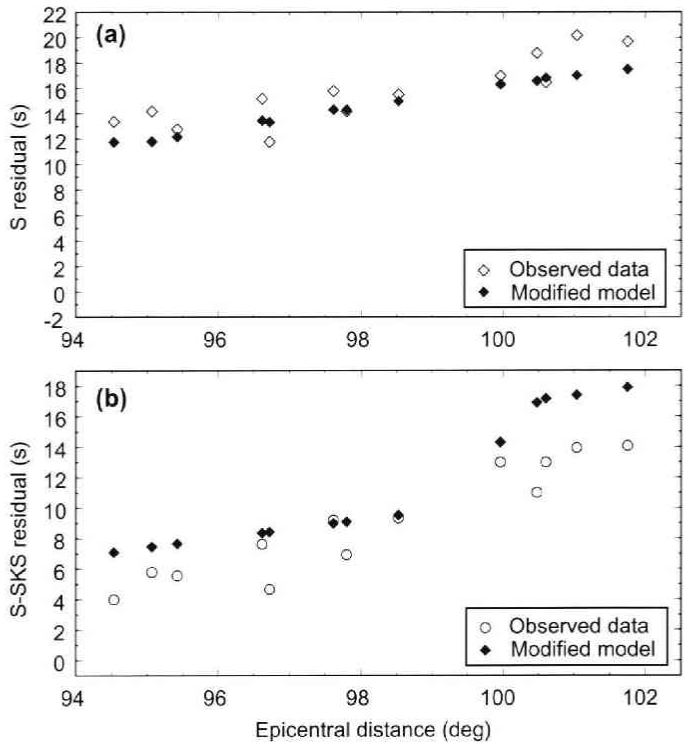

Fig. 8. Comparison between the observed travel time residuals of (a) S and (b) S-SKS with the residuals predicted by the modified model. The proposed model can explain the observed data reasonably well.

sentative depth ranges are (a) 2,891-2,571 km, (b) 2,571-2,271 km, (c) 2,271-2,071 km and (d) 2,071-1,371 km, respectively. In each panel the background remains the S-wave velocity perturbation from SKS12WM13 at the selected depths of (a) 2,750 km, (b) 2,350 km, (c) 2,050 km and (d) 1,750 km to show the distribution of low-velocity anomalies (given in circles). The unmodified regions compared to model SKS12WM13 are illustrated with diamond plots. The African low-velocity region is wider at the base of the mantle (2,891-2,571 km) and mainly dominates beneath the Southeastern Atlantic Ocean with an extension to the continent. In the deeper part of the lower mantle (2,571-2,071 km), the low-velocity region becomes narrower gradually with decreasing depth ranges. In the shallowest depth range (2,071-1,371 km), the low-velocity region is centered progressively further to the northeast concentrating beneath the African continent.

Figs. 10a and 10b show the S-wave velocity perturbations of model SKS12WM13. Fig. 10a shows the perturbations through a whole mantle cross-section connecting the Colombia event to the Kaapvaal array. The great circle paths for S, SKS and SKKS phases from the Colombia event to representative stations of Kaapvaal array are also shown. Fig. 10b displays the perturbations along the great circle paths connecting the

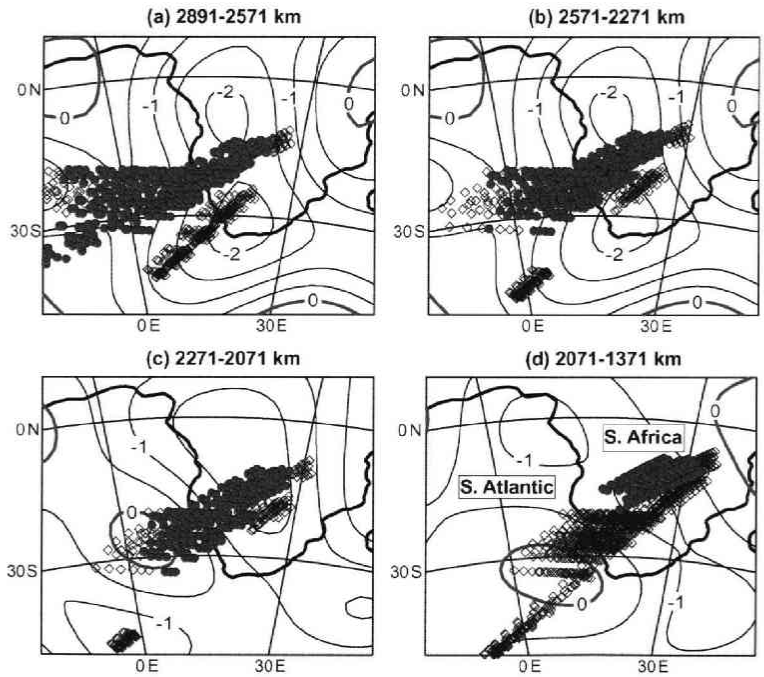

Fig. 9. Shear velocity reduction beneath South Africa. The circles indicate low-velocity regions with 3% S-wave velocity reduction and diamonds denote the unmodified regions compared to model SKS12WM13. The background contour lines show the S-wave velocity perturbations from model SKS12WM13 at depth of (a) 2,750 km, (b) 2,350 km, (c) 2,050 km and (d) 1,750 km. The contour interval is 0.5%. Note that the low velocity region becomes narrower gradually and is centered progressively to the northeast direction of the southwestern Africa with increasing height above the CMB.

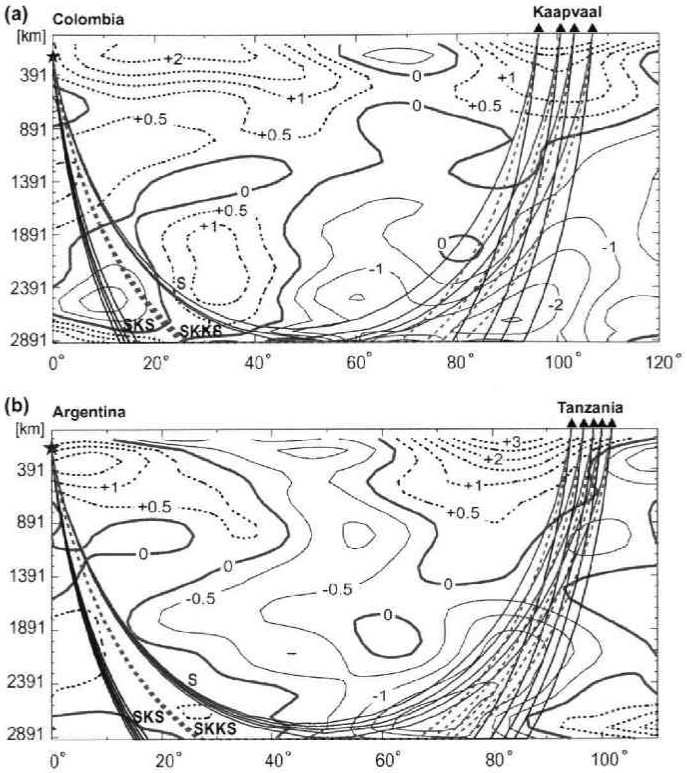

Fig. 10. Shear velocity perturbations from the 3-D mantle model SKS12WM13. (a) A cross section together with the great circle paths for the multiple S phases from the Colombia event to the Kaapvaal array. The horizontal axis represents the distance from the earthquake source. Red, blue and dashed curves indicate the S, SKS and SKKS ray paths, respectively. The Solid contour lines indicate the low-velocity regions, the doted lines denote the fast-velocity region and the green lines indicate a zero perturbation with respect to PREM. Contour interval is 0.5%. Star indicates the Colombia event at 198.7 km focal depth. Triangles denote representative stations of the Kaapvaal array covering the entire distance range of observation (96°-107°). (b) Same as (a) except for the change of cross section along the ray path that connect the Argentina event to the Tanzania array. Star indicates the Argentina event at 164.0 km focal depth. Triangles denote representative stations of the Tanzania array covering the entire distance range of observation (94°-102°).

Argentina event to the Tanzania array. The ray paths of S, SKS and SKKS phases from the Argentina event to representative stations of Tanzania array are shown as well. Our model predicts a low-velocity region in the lower mantle beneath Africa, including the Eastern Atlantic Ocean. The pattern of heterogeneity indicates a rapid decrease of velocity that starts at a depth of about 1,700 km and continues down to the CMB beneath our area of investigation. The ray paths of S, SKS and SKKS phases propagate through the significant low S-wave velocity region in the lower mantle beneath Africa and Eastern Atlantic. Fig. 11 shows the schematic shape of the shear velocity reduction beneath Africa revealed by the present study. This shape results from the combination

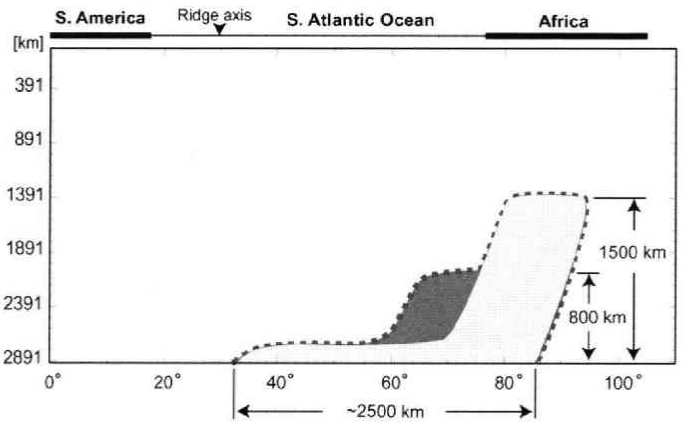

Fig. 11. Schematic illustration of the low-velocity anomaly beneath Africa. The dashed line shows the shape of the anomaly proposed by the present study. In this structure the magnitude of velocity reduction is assumed to be uniformly 3%. The thin line denotes the region of low-velocity anomalies estimated by Ni and Helmberger (2003a, b) with the same velocity reduction. Dark gray area delimits the additionally modified region from the model of Ni and Helmberger. The horizontal axis represents the distance from the epicenter of Argentina event; and the vertical axis represents the depth from the Earth's surface.

of the two different cross-sections described above (see Figs. 10a and 10b). The low-velocity region beneath the Southeastern Atlantic extends up to 800 km above the CMB and therefore it is thicker than that of the previous models (Ni and Helmberger, 2003a, b). The low velocity region may become narrower and extend up to 1,500 km above the CMB under the African continent.

5 Discussions

Here, we concentrate our analysis on the Southern Africa-Atlantic region and investigate the seismic structure by combining the crisscrossing rays. We used teleseismic S and its multiphases recorded by 64 seismic stations belonging to one permanent and two temporary networks in Africa. Differential and absolute travel times of S, ScS, SKS and SKKS phases are used to retrieve the S-wave velocity structure in the lower mantle beneath South Africa. We focus on the data sets obtained from the Argentina (E2) and the Colombia (E3) events in order to introduce a velocity model that can interpret our observations. Applying a forward modeling, a low-velocity region of 800 km depth above the CMB with 3% S-wave velocity reduction beneath the Southwestern Africa to the Southeastern Atlantic is important for explaining the discrepancy between the observed and the theoretical times. The African low velocity region as shown in our proposed model in this study is wider (~2,500 km) at the base of the mantle and mainly dominates beneath the Southeastern Atlantic Ocean extending to the African continent. The low-velocity region beneath the Southeastern Atlantic is thicker than that of the previous models (Ni and Helmberger, 2003a, b). Also, the low-velocity region may

become smaller gradually with respect to the area covering the ray paths and be centered progressively further to the northeast concentrating beneath the African continent.

Ritsema *et al.* (1999) investigated a model of low-velocity region in the lower mantle under the cross-section from the South Sandwich Islands to Tanzania. However, they did not check the SKS12WM13 model. From the Argentina data sets, Ni and Helmberger (2003a, b) proposed a model of S-wave velocity structure with 3% reduction beneath South Africa. This model delimits the region of low-velocity anomalies beneath Atlantic to a thin basal layer of 150 km that extends up to about 1,500 km above the CMB beneath the African continent in the northeast orientation. In addition to the Ni and Helmberger's results, we include Colombia to Kaapvaal, which crisscross the Argentina to Tanzania cross-section. The two different cross-sections including their overlapping seismic phases exit points (see Fig. 1b) provide major contributions in making difference between previous models by Ni and Helmberger (2003a, b) and the present one. This difference results in the modification of the low-velocity region beneath Southeastern Atlantic Ocean up to 800 km thick above the CMB. Also Ni and Helmberger (2003a, b) did not take into account the existing fast velocity anomaly in the upper mantle and crust in the African cratons when absolute times were discussed.

Many factors are candidates contributing to the variations of seismic velocity such as thermal and/or chemical anomalies, partial melting, fluids, cracks, and so forth. Based on the recent results for the partial derivative of seismic velocities with respect to temperature as $\partial \ln Vs/\partial T \approx -45\times10^{-6}\,\mathrm{K}^{-1}$ in the lower mantle (Stacey, 1998), S-wave velocity reduction of 3% can be caused solely by a thermal anomaly with a temperature increase of about 700 K. Since the excess temperature of the mantle plume inferred from buoyancy fluxes are estimated to be about 200 K (Sleep, 1990), temperature anomaly as large as 700 K seems to be too high. Partial melt can reduce effectively the seismic velocity as discussed by Williams and Garnero (1996). Another candidate for S-wave velocity reduction is the increase of iron fraction probably due to the interaction with the outer core at the CMB (Knittle and Jeanloz, 1989). However, such an effect is probably limited near the base of the mantle because that the material which includes iron is dense and may be difficult to extend upward.

The spatial variation of temperature at the CMB may interpret for seismic velocity perturbation. The low-velocity regions are presumably hotter than surrounding regions, and therefore probably represent buoyant upwelling, which become mantle plumes (Anderson, 1981). Recently, Castle *et al.* (2000) and Zhao (2001, 2004) showed that the slow anomalies in the lower mantle down to the CMB correlate well with the hotspots distribution on the Earth's surface, suggesting that the mantle plumes under those hotspots may originate from the CMB. Although the criteria for selection of hotspots are different among the several proposed catalogues, the concentration of hotspots in Africa is common features (Jurdy and Stefanick, 1990). And also an apparent correlation between the partially molten zone and the hot upwellings in the deep Earth is proposed actively by Williams and Garnero (1996). Thus, we infer that the low-velocity anomaly in the lower mantle beneath Africa is probably due to the thermal anomaly of

high temperature and partial melt.

The deflection of plumes due to the influence of mantle flow (Steinberger and O'Connell, 1998; Steinberger, 2000; Zhao, 2001, 2004; Shen *et al.*, 2002) leads to the exhibition of the winding images of the slow anomalies under hotspots. Steinberger (2000) inferred the location of the hotspot roots by tracking plume conduits based on a global mantle flow model and suggested the presence of comparatively broad upwellings rather than localized plumes. This may bring some enlightenment to our understanding on the complex geometry of the low-velocity anomalies imaged beneath Africa.

6 Conclusions

Based on the absolute and differential travel time analyses of S, SKS and SKKS phases, we propose the spatial pattern of the low-velocity anomalies at the lower mantle under the Southern Africa-Atlantic region. While confirming the general view of the lower mantle structure of the region in term of absolute percentage of shear velocity reduction (3%) as done by Ni and Helmberger (2003a, b), we also present important differences in term of the shape of anomalies. This may provide new insights into plume modeling.

Although the methodology is based on traditional ray-theory and the dataset used in the analysis is not very extended, this work represents a modest contribution in delineating the low-velocity structure beneath Southern Africa and Atlantic. Now, the huge low velocity structure has been apparent beneath the Africa and Southeastern Atlantic Ocean. For the precise mapping of seismic heterogeneous structure, an increase in number of new permanent broadband seismic stations is required in Africa and a development of new techniques appropriate for heterogeneous structure is also encouraged.

Acknowledgements

We thank IRIS/DMC for providing the seismic data through the internet. M.K. is grateful to S. Tanaka who provided the program for travel time calculation, useful comments and valuable suggestions throughout this study and thanks A. Hasegawa for his encouragements and suggestions in the course of the study. Thoughtful reviews by D. Zhao, T. Nishimura and an anonymous reviewer helped to improve the manuscript. M.K. is supported by MEXT under the Grant-in-aid from Japanese Government scholarship.

References

Anderson, D.L., 1981: Hot spots, basalts, and the evolution of the mantle, *Science*, **213**, 82-89.

Castle, J.C., K.C. Creager, J.P. Winchester and R.D. van der Hilst, 2000: Shear wave speeds at the base of the mantle, *J. Geophys. Res.*, **105**, B9, 21543-21557.

Choy, G.L. and P.G. Richards, 1975 : Pulse distortion and Hilbert transform in multiply reflected and refracted body waves, *Bull. Seismol. Soc. Am.*, **65**, 1, 55-70.

Courtillot, V., A. Davaille, J. Besse and J. Stock, 2003 : Three distinct types of hotspots in the Earth's mantle, *Earth Planet. Sci. Lett.*, **205**, 295-308.

Dziewonski, A.M. and D.L. Anderson, 1981 : Preliminary reference earth model, *Phys. Earth Planet. Inter.*, **25**, 297-356.

Helmberger, D., S. Ni, L. Wen and J. Ritsema, 2000 : Seismic evidence for ultralow-velocity zones beneath Africa and eastern Atlantic, *J. Geophys. Res.* **105**, B10, 23865-23878.

Jurdy, D.M. and M. Stefanick, 1990 : Models for the hotspot distribution, *Geophys. Res. Lett.*, **17**, 1965 1968.

Kennett, B.L.N. and O. Gudmundsson, 1996 : Ellipticity corrections for seismic phases, *Geophys. J. Int.*, **127**, 40-48.

Knittle, E. and R. Jeanloz, 1989 : Simulating the core-mantle boundary : an experimental study of high-pressure reactions between silicates and liquid iron, *Geophys. Res. Lett.*, **16**, 609-612.

Lavely, E.M., D.W. Forsyth and P. Friedemann, 1986 : Scales of heterogeneity near the core-mantle-boundary, *Geophys. Res. Lett.*, **13**, 1505-1508.

Liu, X.F. and A.M. Dziewonski, 1994 : Lowermost mantle shear wave velocity structure, *EOS, Trans. AGU*, Fall Supplement **75**, 663.

Masters, G., G. Laske, H. Bolton and A. Dziewonski, 2000 : The relative behavior of shear velocity, bulk sound speed, and compressional velocity in the mantle ; Implications for chemical and thermal structure, in Earth's Deep Interior, Mineral physics and tomography from the atomic to the global scale (S.-I.. Karato *et al.*, Eds.), *Geophysical Monograph*, **117**, *Am. Geophys. Un.*, Washington, D.C., 63-67.

Megnin, C. and B. Romanowicz, 2000 : The three-dimensional shear velocity structure of the mantle from the inversion of body, surface and higher-mode waveforms, *Geophys. J. Int.*, **143**, 709-728.

Ni, S., X. Ding, D.V. Helmberger and M. Gurnis, 1999 : Low-velocity structure beneath Africa from forward modeling, *Earth Planet. Sci. Lett.*, **170**, 497-507.

Ni, S. and D.V. Helmberger, 2001a : Horizontal transition from fast to slow structures at the core-mantle boundary, South Atlantic, *Earth Planet. Sci. Lett.*, **187**, 301-310.

Ni, S. and D.V. Helmberger, 2001b : Probing an Ultra-low velocity zone at the core mantle boundary with P and S waves, *Geophys. Res. Lett.*, **28**, 12, 2345-2348.

Ni, S. and D.V. Helmberger, 2003a : Seismological constraints on the South African superplume ; could be the oldest distinct structure on earth, *Earth Planet. Sci. Lett.*, **206**, 119-131.

Ni, S. and D.V. Helmberger, 2003b : Ridge-like lower mantle structure beneath South Africa, *J. Geophys. Res.*, **108**, B2, ESE 12 1-14.

Nyblade, A.A., C. Birt, C.A. Langston, T.J. Owens and R. Last, 1996 : Seismic experiment reveals rifting of craton in Tanzania, *EOS, Trans. AGU*, **77**, 517-521.

Nyblade, A.A. and C.A. Langston, 2002 : Broadband seismic experiments probe the East African rift, *EOS, Trans. AGU*, **83**, 405-408.

Ritsema, J., S. Ni, D.V. Helmberger and H.P. Crotwell, 1998 : Evidence for strong shear velocity reductions and velocity gradients in the lower mantle beneath Africa, *Geophys. Res. Lett.*, **25**, 4245-4248.

Ritsema, J., H.J. van Heijst and J.H. Woodhouse, 1999 : Complex shear wave velocity structure imaged beneath Africa and Iceland, *Science*, **286**, 1925-1928.

Ritsema, J. and R.M. Allen, 2003 : The elusive mantle plume, *Earth Planet. Sci. Lett.*, **207**, 1-12.

Shen, Y., S. Solomon, I. Bjarnason and G. Nolet, 2002 : Seismic evidence for a tilted mantle plume and north-south mantle flow beneath Iceland, *Earth Planet. Sci. Lett.*, **197**, 261-272.

Sleep, N.H., 1990 : Hotspots and mantle plumes : some phenomenology, *J. Geophys. Res.*, **95**, 6715-6736.

Stacey, F.D., 1998 : Thermoelasticity of a mineral composite and a reconsideration of lower mantle properties, *Phys. Earth Planet. Int.*, **106**, 219-236.

Steinberger, B. and R.J. O'Connell, 1998 : Advection of plumes in mantle flow : implications for hotspot motion, mantle viscosity and plume distribution, *Geophys. J. int.*, **132**, 412-434.

Steinberger, B., 2000 : Plumes in a convecting mantle : models and observations for individual hotspots, *J. Geophys. Res.*, **105**, 11127-11152.

Su, W., R.L. Woodward and A.M. Dziewonski, 1994 : Degree 12 model of shear velocity heterogeneity in the mantle, *J. Geophys. Res.*, **99**, 6945-6980.

Tanaka, S. and H. Hamaguchi, 1992 : Heterogeneity in the lower mantle beneath Africa, as revealed from S and ScS phases, *Tectonophysics*, **209**, 213-222.

Williams, Q. and E.J. Garnero, 1996 : Seismic evidence for partial melt at the base of the Earth's mantle, *Science*, **273**, 1528-1530.

Young, J.B., B.W. Presgrave, H. Aichele, D.A. Wiens and E.A. Flinn, 1996 : The Flinn-Engdahl regionalization scheme : the 1995 version, *Phys. Earth Planet. Int.*, **96**, 223-297.

Zhao, D., 2001 : Seismic structure and origin of hotspots and mantle plumes, *Earth Planet. Sci. Lett.*, **192**, 251-265.

Zhao, D., 2004 : Global tomographic images of mantle plumes and subducting slabs : insight into deep Earth dynamics, *Phys. Earth Planet. Int.*, **146**, 3-34.